

Multi-stage Optimization of Community Microgrid Considering Fair Allocation and Risk Management

Haiteng Han, *Member, IEEE*, Xiangchen Jiang, *Student Member, IEEE*, Can Huang, *Senior Member, IEEE*, Chen Wu, Sheng Chen, *Senior Member, IEEE*, Qingxin Shi, *Member, IEEE*, and Zhinong Wei, *Member, IEEE*

Abstract—As renewable energy and environmental protection gain prominence, community microgrid has become crucial for promoting resource sharing and improving energy efficiency. This paper presents a multi-stage optimization strategy of community microgrid considering fair allocation and risk management, utilizing the Vickrey-Clarke-Groves (VCG) mechanism and the glue value-at-risk (GlueVaR) method. The proposed strategy integrates carbon with the collective self-consumption (CSC) framework, using GlueVaR to manage uncertainties in photovoltaic (PV) power generation by balancing economic performance with extreme risk management. Compared with traditional risk management, the GlueVaR method offers a more comprehensive characterization of both tail risks and central tendency, enabling more robust decision-making under uncertainties. The VCG mechanism ensures accurate supply and demand reporting, thereby optimizing resource allocation. The proposed strategy aims to promote fair allocation, enhance community welfare, reduce carbon emissions, and optimize energy utilization. A distributed alternating direction method of multipliers (ADMM) algorithm is employed to improve the computational efficiency and preserve the privacy of community members, making the proposed strategy scalable to various community microgrid sizes. Case studies confirm that the proposed strategy significantly enhances community welfare, reduces carbon emissions, and strengthens system stability and security. Furthermore, by fostering fair and transparent transactions among members, the cohesion of the community is reinforced for long-term sustainability.

Index Terms—Carbon emission, renewable energy, community microgrid, risk management, uncertainty, distributed optimization, resource allocation, Vickrey-Clarke-Groves (VCG).

Manuscript received: April 8, 2025; revised: June 10, 2025; accepted: August 15, 2025. Date of CrossCheck: August 15, 2025. Date of online publication: August 22, 2025.

This work was supported by the National Natural Science Foundation of China (No. 52307090).

This article is distributed under the terms of the Creative Commons Attribution 4.0 International License (<http://creativecommons.org/licenses/by/4.0/>).

H. Han (corresponding author), X. Jiang, C. Wu, S. Chen, and Z. Wei are with the School of Electrical and Power Engineering, Hohai University, Nanjing, China (e-mail: hanht@hhu.edu.cn; jiangxc@hhu.edu.cn; cwusgcc@gmail.com; chenshenghhu@163.com; wzn_nj@263.net).

C. Huang is with the School of Electrical Engineering, Southeast University, Nanjing, China (e-mail: canhuang@seu.edu.cn).

Q. Shi is with the School of Electrical and Electronic Engineering, North China Electric Power University, Beijing, China (e-mail: qshi@ncepu.edu.cn).

DOI: 10.35833/MPCE.2025.000312

I. INTRODUCTION

ESCALATING energy shortages and environmental pollution have intensified the pursuit of sustainable development. With advancements in smart grids and renewable energy technologies, distributed energy systems are becoming increasingly prevalent. More community members are installing distributed generation equipment such as photovoltaic (PV) units and energy storage systems (ESSs), enhancing energy self-sufficiency and enabling participation in transactions [1]. However, it remains challenging to coordinate energy production and consumption within a community amidst a volatile environment. Community energy management emerges as a proactive solution, optimizing the energy consumption while improving energy efficiency and environmental outcomes [2].

The European Union has made considerable strides in advancing sustainable energy development, notably through the issuance of the Clean Energy Package (CEP) [3], which aims to foster a green society. The CEP has enabled the development of community microgrid by supporting energy communities [4], with collective self-consumption (CSC) emerging as a prominent framework. In the CSC framework, community microgrid members (both energy producers and consumers) engage in local production and consumption through sharing mechanisms, thereby lowering energy costs and enhancing resource utilization efficiency [5]. The community microgrid is organized around the *Personne Morale Organisatrice* (PMO), a French term that denotes an entity responsible for managing community activities and liaising with utilities and third-party stakeholders. The CSC framework not only boosts self-sufficiency in energy but also fosters local economic growth and strengthens community bonds. Reference [6] shows that peer-to-peer (P2P) and CSC framework can enhance energy efficiency and grid resilience, while [7] proposes a three-stage strategy of the CSC framework and coordinates the energy consumption within grid limitations for optimization.

It is essential to ensure fairness and efficiency in community microgrid. Traditional electricity scheduling strategies are not always effective in incentivizing accurate supply and demand reporting, risking manipulation, and unfair practices.

While blockchains enhance transparency through decentralized ledgers [8], their high implementation costs may burden resource-limited communities [9]. The Vickrey [10]-Clarke [11]-Groves [12] (VCG) mechanism offers an effective alternative by ensuring truthful bidding through its core principle: each participant pays an amount equal to the externality they impose on others, calculated as the difference between total welfare with and without their participation. The VCG mechanism operates by making truthful reporting of the dominant strategy regardless of actions of other participants, as any misrepresentation will either have no effect or result in less favorable outcomes for the misreporting participant. In community microgrid, this addresses the critical challenge of strategic misreporting in energy demand and supply declarations, where members might otherwise overstate the needs or understate the generation capacity for favorable allocations. The VCG mechanism provides key advantages including incentive compatibility for truthful bidding, individual rationality ensuring no participant loses by participation, and automatic maximization of social welfare. Reference [13] introduces a VCG-based allocation method that deters deceptive behaviors in demand response, promoting fairness and maximizing social welfare. By aligning individual incentives with truthful bidding [14], VCG supports efficient market operations.

Community microgrid continues to face significant challenges, particularly beyond the scope of electricity scheduling. Current research often focuses on basic strategies of local power sharing, neglecting the complexities introduced by high penetration of PVs and ESSs [15]. These factors can cause system fluctuations, adversely impacting grid stability and introducing economic risks. Reference [16] introduces a multi-consumer distributed scheduling strategy based on conditional value-at-risk (CVaR), considering distribution network constraints and uncertainties. Additionally, [17] proposes a dual-layer energy management strategy to coordinate P2P energy trading among multiple consumers, using CVaR to estimate the potential losses of retailers. However, a single risk metric may struggle to balance risk management for extreme events with system flexibility [18].

Existing CSC framework has considerable potential for expansion in carbon quota allocation. Integrating carbon into the CSC framework allows communities to optimize the consumption of renewable energy sources such as PV and wind power, thereby reducing the dependence on fossil fuel and lowering carbon emissions [19]. Participants in carbon quota allocation can generate additional income by selling carbon quotas or offset their emissions by buying the quotas, maximizing economic benefits [20]. This incentivizes communities to cut carbon emissions and enhance energy efficiency, supporting environmental protection and sustainable development [21]. Embedding carbon into the CSC framework could attract greater policy and regulatory support, further advancing the adoption of renewable energy.

Existing research works highlight the need for improvements in community microgrid, particularly in information transparency, risk management, and carbon quota allocation. This paper introduces a multi-stage optimization strategy of

community microgrid considering fair allocation and risk management, utilizing the VCG mechanism and incorporating the glue value-at-risk (GlueVaR) method to quantify and manage risks. The GlueVaR method enables a balanced assessment of both expected and extreme losses under uncertainties by combining the strengths of value-at-risk (VaR) and CVaR. The proposed strategy minimizes operational costs and risk exposure by employing the alternating direction method of multipliers (ADMM) algorithm for distributed computation, which ensures both computational efficiency and privacy protection for community microgrid members. The primary contributions of this paper are described as follows.

1) The VCG mechanism is implemented in allocation to prevent fraudulent behaviors in quantity reporting. During the monthly settlement stage, the VCG mechanism effectively eliminates misreporting, promotes honest fair allocation, and enhances operational efficiency. Furthermore, accurate quantity of reporting contributes to the stable operation of the community microgrid.

2) A GlueVaR method is proposed to address the PV uncertainties for risk management. In the day-ahead stage, GlueVaR captures both average and extreme operational risks associated with PV fluctuations, providing a more balanced and robust measure for risk-aware decision-making.

3) An improved CSC framework is introduced by incorporating carbon quota allocation to enhance the benefits for community microgrid members. Unlike general scheduling, which focuses on overall stability of power grid, the CSC framework emphasizes local energy sharing and direct community welfare, incentivizing renewable adoption and reducing dependence on centralized systems.

This paper is structured as follows. Section II presents the community microgrid models, detailing both the global community microgrid model and local community member model. Section III outlines the proposed strategy of community microgrid considering energy and carbon based on the VCG mechanism. Section IV describes the model solution. Section V presents case studies to evaluate the proposed strategy. Finally, Section VI outlines the conclusion of this paper.

II. COMMUNITY MICROGRID MODELS

This section outlines the community microgrid models used in this paper, categorized into the global community microgrid model and the local community member model based on objects and scope. Figure 1 shows the framework of the community microgrid, illustrating the relationship between community microgrid members and the PMO. In Fig. 1, DSO represents the distribution system operator.

Community microgrid members can interact with each other or with retailers. Prices within the community microgrid are more favorable compared with direct transactions with retailers: selling prices within the community microgrid are higher, and buying prices are lower. Additionally, members actively coordinate with the PMO to address issues in both the day-ahead and real-time stages.

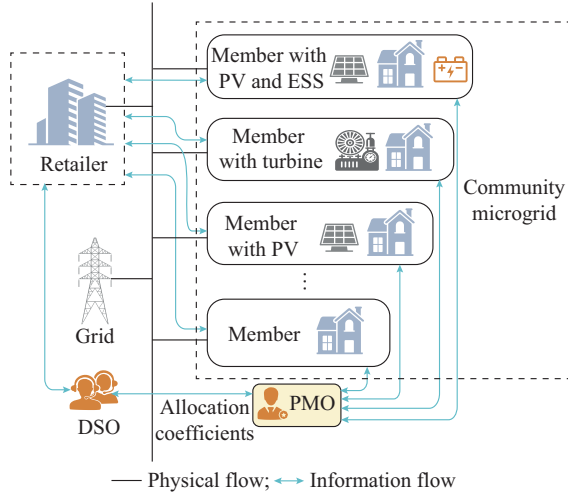


Fig. 1. Framework of community microgrid.

A. Global Community Microgrid Model

In this paper, each community microgrid member engages in autonomous transactions within the community microgrid, submits proposed quantity in the day-ahead stage, and then conducts them in the real-time stage. After the community interaction concludes, the PMO collects data from both stages to assess whether the voltage of community microgrid will exceed the system safety limits. During the monthly settlement stage, the PMO determines the allocation coefficient of each member based on their participation, and submits it to the DSO, which then performs the actual allocation.

The relationship between $p_{i,t}^{\text{lin}}$ and other variables is defined:

$$p_{i,t}^{\text{lin}} = p_{i,t}^{\text{gb}} + p_{i,t}^{\text{cb}} - p_{i,t}^{\text{gs}} - p_{i,t}^{\text{cs}} \quad (1)$$

where $p_{i,t}^{\text{lin}}$ is the line power of member i at time t ; $p_{i,t}^{\text{gb}}$ and $p_{i,t}^{\text{gs}}$ are the electricity bought from and sold to retailers by member i at time t , with prices π_i^{gb} and π_i^{gs} , respectively; and $p_{i,t}^{\text{cb}}$ and $p_{i,t}^{\text{cs}}$ are the electricity bought and sold within the community microgrid by member i at time t , with prices π_i^{cb} and π_i^{cs} , respectively.

It is essential to ensure that the total electricity bought and sold within the community microgrid at any given time t is equal to maintain the balance and safety:

$$\Omega_t = \sum_{i \in \mathcal{U}} p_{i,t}^{\text{cb}} = \sum_{i \in \mathcal{U}} p_{i,t}^{\text{cs}} \quad (2)$$

where Ω_t is the total amount of electricity bought or sold within the community at time t . Based on (2), the allocation coefficients of electricity bought and sold for member i at time t , denoted by $\lambda_{i,t}^{\text{b}}$ and $\lambda_{i,t}^{\text{s}}$, respectively, can be computed as:

$$\begin{cases} \lambda_{i,t}^{\text{b}} = \frac{p_{i,t}^{\text{cb}}}{\Omega_t} \\ \lambda_{i,t}^{\text{s}} = \frac{p_{i,t}^{\text{cs}}}{\Omega_t} \end{cases} \quad (3)$$

These coefficients must satisfy the following condition to ensure that their sum equals 1:

$$\begin{cases} \sum_{i \in \mathcal{U}} \lambda_{i,t}^{\text{b}} = 1 \\ \sum_{i \in \mathcal{U}} \lambda_{i,t}^{\text{s}} = 1 \end{cases} \quad (4)$$

where \mathcal{U} is the set of community microgrid members.

In addition to managing allocation benefits for community microgrid members, the PMO must ensure the voltage stability for individual members and the community microgrid. Therefore, the global community microgrid model must include the transmission network model. The community is connected to a low-voltage distribution network with \mathcal{N} nodes. We then have:

$$i_{ij,t}^2 = I_{ij,t} = \frac{p_{ij,t}^2 + q_{ij,t}^2}{v_{i,t}} \quad (5)$$

where $i_{ij,t}$, $p_{ij,t}$ and $q_{ij,t}$ are the current, active power, and reactive power flowing from bus i to bus j through the resistance r_{ij} and reactance x_{ij} at time t , respectively; and $v_{i,t}$ and $I_{ij,t}$ are the squared voltage at bus i and the squared current on line ij , respectively.

The network equations are expressed using DistFlow model [22] as:

$$p_{ij,t} - p_{j,t}^{\text{lin}} = \sum_{l \in S_j^{\text{b,d}}} p_{jl,t} + r_{ij} I_{ij,t} \quad (6)$$

$$q_{ij,t} - q_{j,t}^{\text{lin}} = \sum_{l \in S_j^{\text{b,d}}} q_{jl,t} + x_{ij} I_{ij,t} \quad (7)$$

$$v_{j,t} = v_{i,t} - 2(p_{ij,t} r_{ij} + q_{ij,t} x_{ij}) + (r_{ij}^2 + x_{ij}^2) I_{ij,t} \quad (8)$$

where $S_j^{\text{b,d}}$ is the set of branches starting at node j . $\sum_{l \in S_j^{\text{b,d}}} p_{jl,t}$ and $\sum_{l \in S_j^{\text{b,d}}} q_{jl,t}$ represent the total active and reactive power flows of all branches connected downstream of node j , respectively.

B. Local Community Member Model

In this paper, the load is non-flexible, meaning that there is no reducible or transferable load. However, some members have PV units and ESSs. This paper includes residential members and some members with gas units, who primarily demand and buy carbon quotas. Community microgrid members are therefore categorized as gas members, PV members, and ESS members.

1) Gas Members

For gas members (members with gas units), the model must account for their output [23].

$$s_{i,t}^{\text{T}} = \eta_{\text{T}} Q_{\text{CH}_4} V_{i,t}^{\text{T}} \quad (9)$$

$$p_{i,t}^{\text{T}} = s_{i,t}^{\text{T}} \cos \theta_i^{\text{T}} \quad (10)$$

$$q_{i,t}^{\text{T}} = s_{i,t}^{\text{T}} \sin \theta_i^{\text{T}} \quad (11)$$

where $s_{i,t}^{\text{T}}$ is the apparent power generated by the gas unit for member i at time t ; η_{T} is the efficiency of the gas unit; Q_{CH_4} is the calorific value of natural gas combustion; $V_{i,t}^{\text{T}}$ is the amount of natural gas consumed by the gas unit for member i at time t ; θ_i^{T} is the power angle of the gas unit; and $p_{i,t}^{\text{T}}$ and $q_{i,t}^{\text{T}}$ are the corresponding active power and reactive power, respectively.

The operational cost of the gas unit $C_{i,t}^{\text{CH}_4}$, determined by gas consumption and natural gas prices $\pi_t^{\text{CH}_4}$, is defined by:

$$C_{i,t}^{\text{CH}_4} = \pi_t^{\text{CH}_4} V_{i,t}^{\text{T}} \quad (12)$$

For members without gas units, $V_{i,t}^{\text{T}}$ is zero; thus, $s_{i,t}^{\text{T}}$, $p_{i,t}^{\text{T}}$ and $q_{i,t}^{\text{T}}$ are also zero.

2) PV Members

PV members must meet the following constraints.

$$0 \leq p_{i,t}^{\text{PV}} \leq \bar{p}_{i,t}^{\text{PV}} \quad (13)$$

$$\left(p_{i,t}^{\text{PV}}\right)^2 + \left(q_{i,t}^{\text{PV}}\right)^2 \leq \left(s_{i,t}^{\text{PV}}\right)^2 \quad (14)$$

$$\left|q_{i,t}^{\text{PV}}\right| \leq p_{i,t}^{\text{PV}} \tan \theta_i^{\text{PV}} \quad (15)$$

where $p_{i,t}^{\text{PV}}$ is the active power generated by the PV unit; $\bar{p}_{i,t}^{\text{PV}}$ is the upper limit of PV output; $s_{i,t}^{\text{PV}}$ and $q_{i,t}^{\text{PV}}$ are the apparent and reactive power generated by the PV unit, respectively; and θ_i^{PV} is the power angle of the PV unit.

3) ESS Members

For ESS members, the state of charge (SOC) must be considered. The SOC during the charging and discharging processes of member i at time t is $SOC_{i,t}$. We have:

$$SOC_{i,t+\Delta t} = SOC_{i,t} + \left(\eta^{\text{ch}} p_{i,t}^{\text{ch}} - \frac{p_{i,t}^{\text{dis}}}{\eta^{\text{dis}}}\right) \Delta t \quad (16)$$

$$SOC_i^{\mathcal{T}_d} = SOC_i^0 \quad (17)$$

$$p_{i,t}^{\text{B}} = p_{i,t}^{\text{ch}} - p_{i,t}^{\text{dis}} \quad (18)$$

where $p_{i,t}^{\text{ch}}$ and $p_{i,t}^{\text{dis}}$ are the charging power and discharging power of member i at time t , respectively; η^{ch} and η^{dis} are the charging and discharging efficiencies, respectively; $p_{i,t}^{\text{B}}$ is the net power of the battery at time t ; and the SOC at the

end of the scheduling horizon ($SOC_i^{\mathcal{T}_d}$) is required to equal that at the beginning (SOC_i^0), ensuring energy neutrality within each operation period. \mathcal{T}_d is the 30 min interval in the day-ahead stage. The SOC is constrained by its maximum capacity \overline{SOC}_i and minimum capacity \underline{SOC}_i , and the charging power and discharging power are also limited by $\bar{p}_{i,t}^{\text{ch}}$ and $\bar{p}_{i,t}^{\text{dis}}$, respectively.

$$\underline{SOC}_i \leq SOC_{i,t} \leq \overline{SOC}_i \quad (19)$$

$$0 \leq p_{i,t}^{\text{ch}} \leq \bar{p}_{i,t}^{\text{ch}} \quad (20)$$

$$0 \leq p_{i,t}^{\text{dis}} \leq \bar{p}_{i,t}^{\text{dis}} \quad (21)$$

Finally, the balance of active and reactive power transmission also needs to be considered [24] as:

$$p_{i,t}^{\text{lin}} = p_{i,t}^{\text{load}} + p_{i,t}^{\text{B}} - p_{i,t}^{\text{PV}} - p_{i,t}^{\text{T}} \quad (22)$$

$$q_{i,t}^{\text{lin}} = q_{i,t}^{\text{load}} + q_{i,t}^{\text{B}} - q_{i,t}^{\text{PV}} - q_{i,t}^{\text{T}} \quad (23)$$

$$\left(p_{i,t}^{\text{lin}}\right)^2 + \left(q_{i,t}^{\text{lin}}\right)^2 \leq \left(s_{i,t}^{\text{lin}}\right)^2 \quad (24)$$

where $p_{i,t}^{\text{load}}$ and $q_{i,t}^{\text{load}}$ are the active and reactive power demands of member i at time t , respectively. $p_{i,t}^{\text{PV}}$, $p_{i,t}^{\text{B}}$, $q_{i,t}^{\text{PV}}$, and $q_{i,t}^{\text{B}}$ remain zero for members without PV units or ESSs.

III. PROPOSED STRATEGY OF COMMUNITY MICROGRID

This section models the community microgrid members and PMO based on the descriptions in Section II. The community interaction is divided into three stages (I-III): day-ahead management, real-time adjustment, and monthly settlement, each addressing different issues. Figure 2 illustrates the proposed strategy of community microgrid, where OPF represents the optimal power flow.

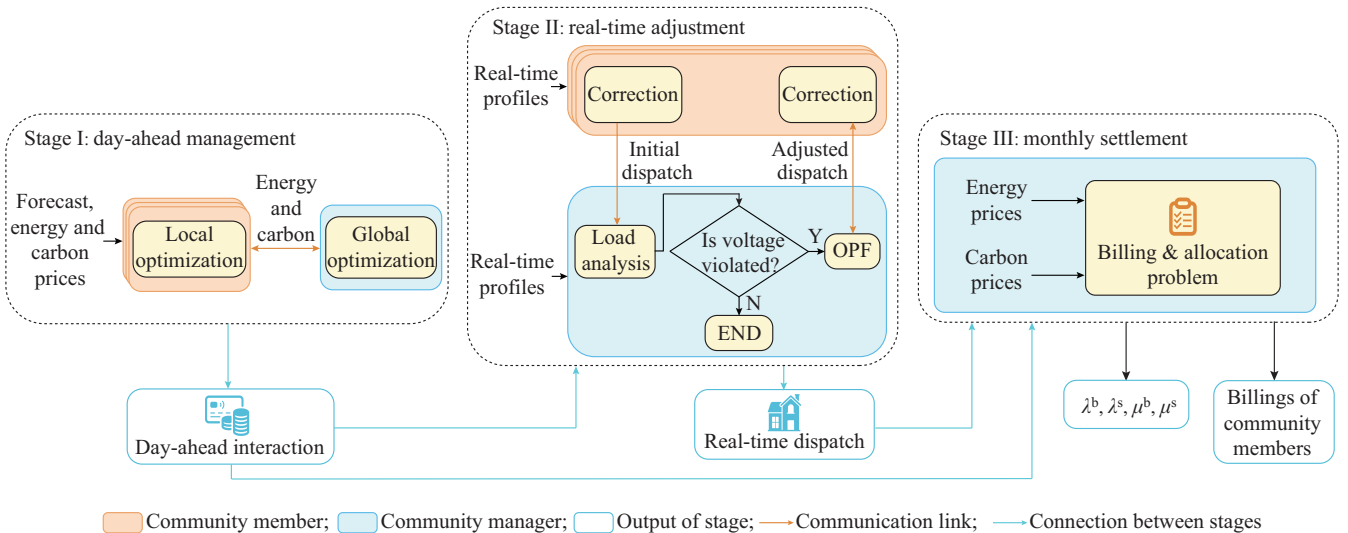


Fig. 2. Proposed strategy of community microgrid.

A. Stage I: Day-ahead Management

In Stage I, each member submits planned energy transactions for the following day to the PMO. The PMO then estimates and allocates these transactions to minimize costs for members. Reactive power and grid models are excluded in this stage to simplify computations.

To maximize the benefits for members with renewable energy generation units, the CSC framework is enhanced. In this stage, community microgrid members can utilize carbon quotas in addition to electricity. They can buy carbon quotas or sell excess ones based on their usage. A specific amount of carbon quotas [25] $w_{i,t}^0$ is allocated to each member with a

generation unit, determined by their installed capacity:

$$w_{i,t}^0 = D(p_{i,t}^{\text{PV}} + p_{i,t}^{\text{B}} + p_{i,t}^{\text{T}}) \quad (25)$$

where D is the carbon quota allocation coefficient, which determines the amount of carbon quotas granted per unit of installed generation capacity.

The gas units emit a specific amount of CO_2 during power generation calculated by:

$$w_{i,t}^{\text{CO}_2} = \alpha p_{i,t}^{\text{T}} \quad (26)$$

where α is the carbon emission factor of gas units, representing the amount of CO_2 emissions per unit of electricity generated by the gas turbine.

Consequently, the required carbon quota buying or selling quantities, denoted by $w_{i,t}^{\text{CO}_2^{\text{b}}}$ and $w_{i,t}^{\text{CO}_2^{\text{s}}}$, respectively, can be determined:

$$w_{i,t}^{\text{CO}_2^{\text{b}}} = \max(w_{i,t}^{\text{CO}_2} - w_{i,t}^0, 0) \quad (27)$$

$$w_{i,t}^{\text{CO}_2^{\text{s}}} = \max(w_{i,t}^0 - w_{i,t}^{\text{CO}_2}, 0) \quad (28)$$

where $w_{i,t}^0$, $w_{i,t}^{\text{CO}_2}$, $w_{i,t}^{\text{CO}_2^{\text{b}}}$, and $w_{i,t}^{\text{CO}_2^{\text{s}}}$ are zero for members without generation units.

$$C_{i,t}^{\text{buy}} = p_{i,t}^{\text{gbDA}} \pi_t^{\text{gb}} + p_{i,t}^{\text{cbDA}} \pi_t^{\text{cbDA}} \quad (29)$$

$$C_{i,t}^{\text{CO}_2^{\text{buy}}} = w_{i,t}^{\text{CO}_2^{\text{cb}}} \pi_t^{\text{cbCO}_2} + w_{i,t}^{\text{CO}_2^{\text{gb}}} \pi_t^{\text{gbCO}_2} \quad (30)$$

$$R_{i,t}^{\text{sell}} = p_{i,t}^{\text{gsDA}} \pi_t^{\text{gs}} + p_{i,t}^{\text{csDA}} \pi_t^{\text{cs}} \quad (31)$$

$$R_{i,t}^{\text{CO}_2^{\text{sell}}} = w_{i,t}^{\text{CO}_2^{\text{cs}}} \pi_t^{\text{csCO}_2} + w_{i,t}^{\text{CO}_2^{\text{gs}}} \pi_t^{\text{gsCO}_2} \quad (32)$$

where $C_{i,t}^{\text{buy}}$ is the electricity buying cost for member i at time t ; $C_{i,t}^{\text{CO}_2^{\text{buy}}}$ is the carbon buying cost; $R_{i,t}^{\text{sell}}$ is the electricity selling revenue; $R_{i,t}^{\text{CO}_2^{\text{sell}}}$ is the carbon quota selling revenue; $p_{i,t}^{\text{cbDA}}$ and $p_{i,t}^{\text{gbDA}}$ are the electricity bought within the community microgrid and from retailer by member i at time t during the day-ahead stage, respectively; $w_{i,t}^{\text{CO}_2^{\text{cb}}}$ and $w_{i,t}^{\text{CO}_2^{\text{gb}}}$ are the carbon quotas bought within the community microgrid and from retailer by member i at time t , respectively; $\pi_t^{\text{cbCO}_2}$ and $\pi_t^{\text{gbCO}_2}$ are the prices for buying and selling carbon quotas within the community microgrid for carbon quota allocation, respectively; $p_{i,t}^{\text{gsDA}}$ and $p_{i,t}^{\text{csDA}}$ are the electricity sold to retailer and within the community microgrid by member i at time t in the day-ahead stage, respectively; $w_{i,t}^{\text{CO}_2^{\text{cs}}}$ and $w_{i,t}^{\text{CO}_2^{\text{gs}}}$ are the carbon quotas sold within the community microgrid and to retailer by member i at time t , respectively; and $\pi_t^{\text{gsCO}_2}$ and $\pi_t^{\text{csCO}_2}$ are the prices for buying and selling carbon quotas with external entities, respectively.

In this stage, each community microgrid member seeks to minimize operational costs, as defined by the following objective function:

$$\begin{cases} \min_{x_i^{\text{DA}}} f_i^{\text{DA}} = \sum_{t \in \mathcal{T}_d} (C_{i,t}^{\text{buy}} + C_{i,t}^{\text{CO}_2^{\text{buy}}} + C_{i,t}^{\text{CH}_4} - R_{i,t}^{\text{sell}} - R_{i,t}^{\text{CO}_2^{\text{sell}}}) \Delta t_d \\ \text{s.t. (1), (9)-(22), (25)-(28)} \end{cases} \quad (33)$$

where the day-ahead decision variable x_i^{DA} comprises $p_{i,t}^{\text{ch}}$, $p_{i,t}^{\text{dis}}$, $\text{SOC}_{i,t}$, $p_{i,t}^{\text{gb}}$, $p_{i,t}^{\text{cb}}$, $w_{i,t}^{\text{CO}_2^{\text{b}}}$, $p_{i,t}^{\text{gs}}$, $p_{i,t}^{\text{cs}}$ and $w_{i,t}^{\text{CO}_2^{\text{s}}}$; and Δt_d is the time interval of each day-ahead step.

To account for PV uncertainties, which may impact system operation and pose certain risks to community schedul-

ing, several multiple scenarios are generated from historical PV data, where \mathcal{S} is the set of scenarios. The objective function for each member is then defined as:

$$\begin{cases} \min_{x_i^{\text{DA}}} f_i^{\text{DA}} = \sum_{k \in \mathcal{S}} \sum_{t \in \mathcal{T}_d} \phi_k (C_{i,t}^{\text{buy}} + C_{i,t}^{\text{CO}_2^{\text{buy}}} + C_{i,t}^{\text{CH}_4} - R_{i,t}^{\text{sell}} - R_{i,t}^{\text{CO}_2^{\text{sell}}}) \Delta t_d \\ \text{s.t. (1), (9)-(22), (25)-(28)} \end{cases} \quad (34)$$

where ϕ_k is the probability of each scenario.

While CVaR provides a coherent risk management by considering the expected value of losses beyond the VaR threshold, it has limitations in capturing the full risk profile. CVaR focuses primarily on tail risks at a single confidence level, which can be overly conservative at high confidence levels or insufficient for extreme events at moderate confidence levels. To overcome these limitations, this paper adopts GlueVaR, which integrates two CVaRs and one VaR at different confidence levels α and β , with α typically reflecting moderate deviations and β addressing more severe risk events. In contrast to the single threshold of CVaR, GlueVaR enables multi-dimensional risk management across different confidence levels, allowing for flexible risk preferences through adjustable weights, as illustrated in (37). This comprehensive risk management, combined with improved economic efficiency, makes GlueVaR particularly well-suited to community microgrid that faces significant uncertainties from renewable energy sources. The formulation of GlueVaR is expressed as:

$$C_i^{\text{GlueVaR}} = \omega_1 C_i^{\text{CVaR}_\beta} + \omega_2 C_i^{\text{CVaR}_\alpha} + \omega_3 C_i^{\text{VaR}_\alpha} \quad (35)$$

$$C_i^{\text{CVaR}_\alpha} = C_i^{\text{VaR}_\alpha} + \frac{1}{1-\alpha} \sum_k \phi_k z_{i,k}^\alpha \quad (36)$$

$$C_i^{\text{CVaR}_\beta} = C_i^{\text{VaR}_\beta} + \frac{1}{1-\beta} \sum_k \phi_k z_{i,k}^\beta \quad (37)$$

where C_i^{GlueVaR} is the GlueVaR cost of member i ; $C_i^{\text{CVaR}_\alpha}$ and $C_i^{\text{CVaR}_\beta}$ are the CVaR costs of member i at confidence levels of α and β , respectively; $0 \leq \alpha < \beta \leq 1$; $C_i^{\text{VaR}_\alpha}$ is the VaR cost of member i at confidence level α ; $\omega_1, \omega_2, \omega_3$ are the weights, $\omega_3 = 1 - \omega_1 - \omega_2$; and $z_{i,k}^\alpha$ and $z_{i,k}^\beta$ are the slack variables. By adjusting the weights ω_1 and ω_2 , GlueVaR can represent any risk measure within the range of both VaR and CVaR [26].

To implement GlueVaR in the day-ahead stage, an equivalent reformulation is introduced using auxiliary variables. The CVaR terms at confidence levels α and β are linearized by introducing $z_{i,k}^\alpha$ and $z_{i,k}^\beta$, which capture the cost excess over the corresponding VaR thresholds in scenario k . The resulting constraint set is defined as:

$$\begin{cases} z_{i,k}^\alpha \geq 0 \\ z_{i,k}^\beta \geq 0 \end{cases} \quad (38)$$

$$z_{i,k}^\alpha \geq \sum_t (C_{i,t,k}^{\text{buy}} + C_{i,t,k}^{\text{CO}_2^{\text{buy}}} - R_{i,t,k}^{\text{sell}} - R_{i,t,k}^{\text{CO}_2^{\text{sell}}}) - C_i^{\text{VaR}_\alpha} \quad (39)$$

$$z_{i,k}^\beta \geq \sum_t (C_{i,t,k}^{\text{buy}} + C_{i,t,k}^{\text{CO}_2^{\text{buy}}} - R_{i,t,k}^{\text{sell}} - R_{i,t,k}^{\text{CO}_2^{\text{sell}}}) - C_i^{\text{VaR}_\beta} \quad (40)$$

The GlueVaR-based model can be expressed as:

$$\begin{cases} \min_{x_i^{\text{DA}}} \left[(1-L_i) f_i^{\text{DA}} + L_i C_i^{\text{GlueVaR}} \right] \\ \text{s.t. (1), (9)-(22), (25)-(28), (37)-(40)} \end{cases} \quad (41)$$

where L_i is the risk preference indicating the risk aversion of members, with values ranging within $[0, 1]$. Higher L_i values indicate higher risk aversion, i. e., more emphasis on risk management rather than on cost minimization.

Upon solving their optimization problems, community microgrid members submit their proposed volumes to the PMO, which then verifies and adjusts them to minimize the overall costs while ensuring balance in the community microgrid.

With carbon incorporated in this stage, the PMO must account for carbon balance constraints and establish the allocation coefficients for buying and selling:

$$\Phi_t = \sum_{i \in \mathcal{U}} w_{i,t}^{\text{CO}_2\text{b}} = \sum_{i \in \mathcal{U}} w_{i,t}^{\text{CO}_2\text{s}} \quad (42)$$

$$\begin{cases} \mu_{i,t}^{\text{b}} = \frac{w_{i,t}^{\text{CO}_2\text{b}}}{\Phi_t} \\ \mu_{i,t}^{\text{s}} = \frac{w_{i,t}^{\text{CO}_2\text{s}}}{\Phi_t} \end{cases} \quad (43)$$

$$\begin{cases} \sum_{i \in \mathcal{U}} \mu_{i,t}^{\text{b}} = 1 \\ \sum_{i \in \mathcal{U}} \mu_{i,t}^{\text{s}} = 1 \end{cases} \quad (44)$$

Consequently, the optimization problem in the first stage is:

$$\begin{cases} \min_{x^{\text{DA}}} f_g^{\text{DA}} = \sum_{i \in \mathcal{U}} \sum_{t \in \mathcal{T}_d} \left(C_{i,t}^{\text{buy}} + C_{i,t}^{\text{CO}_2\text{buy}} + C_{i,t}^{\text{CH}_4} - R_{i,t}^{\text{sell}} - R_{i,t}^{\text{CO}_2\text{sell}} \right) \Delta t_d \\ \text{s.t. (2), (42)} \end{cases} \quad (45)$$

B. Stage II: Real-time Adjustment and Voltage Regulation

This stage focuses on real-time control of community microgrid constraints, addressing the gaps left by the previous stage, in which these constraints are not accounted for. To mitigate uncertainties, the goal in this stage is to minimize deviations between the proposed and actual quantities. Carbon is excluded from this stage due to its longer time period, which is incompatible with the requirements of real-time response.

Stage II is divided into two parts: correcting deviations between stage I and stage II, and addressing the voltage violations.

First, community microgrid members use devices such as ESSs to make adjustments, minimizing deviations between actual and proposed volumes. This is represented by:

$$SOC_{i,t}^{\text{DA}} - \delta_{\text{SOC}} \leq SOC_{i,t}^{\text{RT}^0} \leq SOC_{i,t}^{\text{DA}} + \delta_{\text{SOC}} \quad (46)$$

where $SOC_{i,t}^{\text{DA}}$ is the day-ahead state of charge of member i at time t ; δ_{SOC} is the tolerance of allowed SOC deviation; and $SOC_{i,t}^{\text{RT}^0}$ is the initial real-time state of charge of member i at time t .

Each member addresses the correction problem to minimize deviations, and submits the initial power $p_{i,t}^{\text{linRT}^0}$ to the

PMO.

$$\begin{cases} \min_{x_i^{\text{RT}^0}} \left(p_{i,t}^{\text{linDA}} - p_{i,t}^{\text{linRT}^0} \right)^2 \\ \text{s.t. (9)-(24), (46)} \end{cases} \quad (47)$$

where $p_{i,t}^{\text{linDA}}$ is the day-ahead line power of member i at time t ; and $x_i^{\text{RT}^0}$ is the initial decision variable in the real-time stage that comprises $p_{i,t}^{\text{lin}}, p_{i,t}^{\text{PV}}, q_{i,t}^{\text{PV}}, p_{i,t}^{\text{ch}}, p_{i,t}^{\text{dis}}, SOC_{i,t}$ and $q_{i,t}^{\text{B}}$.

The PMO collects and verifies the initial decision variables $x_i^{\text{RT}^0}$ from community microgrid members. If no voltage violations are detected, the submitted power meets the requirements $p_{i,t}^{\text{linRT}} = p_{i,t}^{\text{linRT}^0}$, and no further adjustments are needed.

If the PMO detects voltage violations, where $p_{i,t}^{\text{linRT}} \neq p_{i,t}^{\text{linRT}^0}$, the problem becomes a multi-objective optimal power flow issue, which can be optimized using second-order cone programming (SOCP) [27].

During voltage adjustments, each member submits new power $p_{i,t}^{\text{linRT}}$ to the PMO. This local optimization problem for each member involves decision variables x_i^{RT} similar to the overall set of all decision variables $x_i^{\text{RT}^0}$. The objective function and constraints are given as:

$$\begin{cases} \min_{x_i^{\text{RT}}} f_i^{\text{RT}} = \left(p_{i,t}^{\text{linDA}} - p_{i,t}^{\text{linRT}} \right)^2 \\ \text{s.t. (9)-(24), (46)} \end{cases} \quad (48)$$

Each community microgrid member aims to minimize the deviations from the scheduled values.

After members complete adjustments, the PMO solves the optimization problem to verify the new quantities and reduce voltage violations across the community microgrid. To facilitate solving the problem, (5) is relaxed to (49) by SOCP. Voltage limits are imposed to ensure safe operation, as shown in (50).

$$I_{ij,t} \geq \frac{p_{ij,t}^2 + q_{ij,t}^2}{v_{i,t}} \quad \forall (i,j) \quad (49)$$

$$\bar{v}_{i,t}^2 \geq v_{i,t} \geq \underline{v}_{i,t}^2 \quad \forall i \quad (50)$$

where $\underline{v}_{i,t} = 0.95$ p.u. and $\bar{v}_{i,t} = 1.05$ p.u. are the lower and upper limits of $v_{i,t}$, respectively.

The problem of the PMO involves the following objective function and constraints:

$$\begin{cases} \min_{X^{\text{RT}}} f_g^{\text{RT}} = \sum_{i \in \mathcal{U}} \left(p_{i,t}^{\text{linDA}} - p_{i,t}^{\text{linRT}} \right)^2 + \sum_{(i,j) \in \mathcal{U}} I_{ij,t} r_{ij} \\ \text{s.t. (6), (22)-(24), (49), (50)} \end{cases} \quad (51)$$

where X^{RT} is the variable set for the objective function; and $p_{i,t}^{\text{linRT}}$ is the real-time line power injection of member i at time t . The objective function minimizes the overall community deviations between operations in day-ahead and real-time stages as well as the grid losses.

C. Stage III: Monthly Settlement

At the end of each month, the PMO allocates community energy and carbon quota to each member based on Stages I

and II. By determining the allocation coefficients, the total cost for each member is calculated.

Energy scheduling costs are computed based on real-time transactions, with allocation coefficients updated every 30 min. The energy bought and sold by community microgrid members during this interval is determined as the real-time average as:

$$\begin{cases} P_{i,t}^b = \frac{1}{|\tau_t|} \sum_{t \in \tau_t} \max(0, p_{i,t}^{\text{linRT}}) \\ P_{i,t}^s = \frac{1}{|\tau_t|} \sum_{t \in \tau_t} \min(0, p_{i,t}^{\text{linRT}}) \end{cases} \quad (52)$$

where $P_{i,t}^b$ and $P_{i,t}^s$ are the average buying power and selling power of member i over the 30 min interval, respectively; and τ_t is the interval between t and $t + \Delta t_d - \Delta t_r$, and Δt_r is the duration of real-time interval.

The total actual energy available for distribution at time t is [7] expressed as:

$$\Omega_t = \min \left(\sum_{i \in \mathcal{U}} P_{i,t}^b, \sum_{i \in \mathcal{U}} P_{i,t}^s \right) \quad (53)$$

where Ω_t is the total distributed energy that aligns with the buying and selling.

The carbon quota allocation differs from energy allocation as carbon trading is not considered in the real-time stage due to its longer settlement period. Therefore, the carbon quota quantities are determined based on the results of day-ahead stage, and averaged over the day-ahead time intervals as:

$$\begin{cases} W_{i,t}^{\text{CO}_2^b} = \frac{1}{|\tau_d|} \sum_{t \in \tau_d} w_{i,t}^{\text{CO}_2^b} \\ W_{i,t}^{\text{CO}_2^s} = \frac{1}{|\tau_d|} \sum_{t \in \tau_d} w_{i,t}^{\text{CO}_2^s} \\ \Phi_t = \min \left(\sum_{i \in \mathcal{U}} W_{i,t}^{\text{CO}_2^b}, \sum_{i \in \mathcal{U}} W_{i,t}^{\text{CO}_2^s} \right) \end{cases} \quad (54)$$

where $W_{i,t}^{\text{CO}_2^b}$ and $W_{i,t}^{\text{CO}_2^s}$ are the average carbon quota buying and selling quantities of member i at time t , respectively; and τ_d is the set of day-ahead time intervals.

However, some community microgrid members may engage in fraudulent behaviors to increase profits. Stage II aims to minimize deviations between operations in day-ahead and real-time stages, enhancing grid safety and indirectly deterring fraud, as excessive reporting may lead to voltage violations. Nevertheless, this does not fully eradicate the fraud, as fraudulent reports may not always violate voltage constraints of a member but can still impact other members. To eliminate fraudulent behaviors, ensure fair allocation, and incentivize honest transactions, this paper employs the VCG mechanism for adjustments and corrections during the monthly settlement.

The VCG mechanism is described as follows [28].

First, the utility of community microgrid member i at time t is calculated separately for energy trading and carbon quota trading as:

$$\begin{cases} u_{i,t}^b = P_{i,t}^b - \lambda_{i,t}^b \Omega_t \\ u_{i,t}^s = P_{i,t}^s - \lambda_{i,t}^s \Omega_t \\ u_{i,t}^{\text{CO}_2^b} = W_{i,t}^{\text{CO}_2^b} - \mu_{i,t}^b \Phi_t \\ u_{i,t}^{\text{CO}_2^s} = W_{i,t}^{\text{CO}_2^s} - \mu_{i,t}^s \Phi_t \end{cases} \quad (55)$$

where $u_{i,t}^b$ and $u_{i,t}^s$ are the utilities of member i at time t for buying and selling in energy trading, respectively; and $u_{i,t}^{\text{CO}_2^b}$ and $u_{i,t}^{\text{CO}_2^s}$ are the utilities of member i at time t for buying and selling in carbon quota trading, respectively.

Next, the total utility excluding member i (denoted by subscript “- i ”) is determined for both energy and carbon quota trading as:

$$\begin{cases} u_{-i,t}^b = \sum_{j \in \mathcal{U}, j \neq i} (P_{j,t}^b - \lambda_{j,t}^b \Omega_t) \\ u_{-i,t}^s = \sum_{j \in \mathcal{U}, j \neq i} (P_{j,t}^s - \lambda_{j,t}^s \Omega_t) \\ u_{-i,t}^{\text{CO}_2^b} = \sum_{j \in \mathcal{U}, j \neq i} (W_{j,t}^{\text{CO}_2^b} - \mu_{j,t}^b \Phi_t) \\ u_{-i,t}^{\text{CO}_2^s} = \sum_{j \in \mathcal{U}, j \neq i} (W_{j,t}^{\text{CO}_2^s} - \mu_{j,t}^s \Phi_t) \end{cases} \quad (56)$$

The actual contribution of member i under the VCG mechanism (denoted by superscript VCG) is computed for energy and carbon quota trading as:

$$\begin{cases} u_{i,t}^{\text{VCG}^b} = \sum_{i \in \mathcal{U}} u_{i,t}^b - u_{-i,t}^b \\ u_{i,t}^{\text{VCG}^s} = \sum_{i \in \mathcal{U}} u_{i,t}^s - u_{-i,t}^s \\ u_{i,t}^{\text{VCGCO}_2^b} = \sum_{i \in \mathcal{U}} u_{i,t}^{\text{CO}_2^b} - u_{-i,t}^{\text{CO}_2^b} \\ u_{i,t}^{\text{VCGCO}_2^s} = \sum_{i \in \mathcal{U}} u_{i,t}^{\text{CO}_2^s} - u_{-i,t}^{\text{CO}_2^s} \end{cases} \quad (57)$$

Finally, the corresponding allocation coefficients are calculated for energy and carbon quotas as:

$$\begin{cases} \lambda_{i,t}^{\text{VCG}^b} = \frac{u_{i,t}^{\text{VCG}^b}}{\sum_{i \in \mathcal{U}} u_{i,t}^b} \\ \lambda_{i,t}^{\text{VCG}^s} = \frac{u_{i,t}^{\text{VCG}^s}}{\sum_{i \in \mathcal{U}} u_{i,t}^s} \\ \mu_{i,t}^{\text{VCG}^b} = \frac{u_{i,t}^{\text{VCGCO}_2^b}}{\sum_{i \in \mathcal{U}} u_{i,t}^{\text{CO}_2^b}} \\ \mu_{i,t}^{\text{VCG}^s} = \frac{u_{i,t}^{\text{VCGCO}_2^s}}{\sum_{i \in \mathcal{U}} u_{i,t}^{\text{CO}_2^s}} \end{cases} \quad (58)$$

The VCG mechanism, a truth-inducing mechanism for optimal solutions in community microgrid, effectively incentivizes accurate reporting from community microgrid members. Settlements are based on the marginal contribution of each member to the overall welfare. Members are motivated to report truthfully, as misreporting can lead to less optimal allocations. Overstating demand diminishes the benefits of others and lowers payments, while understating demand increases the cost and payments. Reporting accurate energy demand

and supply is the optimal strategy, regardless of actions of others [29]. This paper focuses on individual fraudulent reports instead of the collusion among multiple members.

The cost for each community microgrid member i at time t is determined according to Ω_t and Φ_t . The internal scheduling costs $C_{i,t}^{\text{cmE}}$ and $C_{i,t}^{\text{cmCO}_2}$ rely on the allocation coefficients $\lambda_{i,t}^b$ and $\lambda_{i,t}^s$ for energy, and $\mu_{i,t}^b$ and $\mu_{i,t}^s$ for carbon quotas, respectively:

$$\begin{cases} C_{i,t}^{\text{cmE}} = (\lambda_{i,t}^{\text{VCGb}} \Omega_t \pi_t^{\text{cb}} - \lambda_{i,t}^{\text{VCGs}} \Omega_t \pi_t^{\text{cs}}) \delta_{im} \\ C_{i,t}^{\text{cmCO}_2} = (\mu_{i,t}^{\text{VCGb}} \Phi_t \pi_t^{\text{cbCO}_2} - \mu_{i,t}^{\text{VCGs}} \Phi_t \pi_t^{\text{csCO}_2}) \delta_{im} \end{cases} \quad (59)$$

where δ_{im} is the monthly settlement time interval. The costs with retailers $C_{i,t}^{\text{gdE}}$ and $C_{i,t}^{\text{gdCO}_2}$ for energy and carbon quotas, respectively, are expressed as:

$$\begin{cases} C_{i,t}^{\text{gdE}} = [(P_{i,t}^b - \lambda_{i,t}^{\text{VCGb}} \Omega_t) \pi_t^{\text{gb}} - (P_{i,t}^s - \lambda_{i,t}^{\text{VCGs}} \Omega_t) \pi_t^{\text{gs}}] \delta_{im} \\ C_{i,t}^{\text{gdCO}_2} = [(W_{i,t}^{\text{CO}_2\text{b}} - \mu_{i,t}^{\text{VCGb}} \Phi_t) \pi_t^{\text{gbCO}_2} - (W_{i,t}^{\text{CO}_2\text{s}} - \mu_{i,t}^{\text{VCGs}} \Phi_t) \pi_t^{\text{gsCO}_2}] \delta_{im} \end{cases} \quad (60)$$

The total energy scheduling cost $C_{i,t}^{\text{td}}$ is formulated as:

$$\begin{cases} C_{i,t}^{\text{td}} = C_{i,t}^{\text{cm}} + C_{i,t}^{\text{gd}} \\ C_{i,t}^{\text{cm}} = C_{i,t}^{\text{cmE}} + C_{i,t}^{\text{cmCO}_2} \\ C_{i,t}^{\text{gd}} = C_{i,t}^{\text{gdE}} + C_{i,t}^{\text{gdCO}_2} \end{cases} \quad (61)$$

To assess the fairness of the allocation method, this paper employs Jain's fairness index [30] to measure fairness. Jain's fairness index for buying and selling is defined as:

$$\begin{cases} I_{\text{Jain}}^b = \frac{\left(\sum_{i=1}^N P_i^b \right)^2}{N \sum_{i=1}^N (P_i^b)^2} \\ I_{\text{Jain}}^s = \frac{\left(\sum_{i=1}^N P_i^s \right)^2}{N \sum_{i=1}^N (P_i^s)^2} \end{cases} \quad (62)$$

where N is the total number of community microgrid members; P_i^b and P_i^s are the average buying power and selling power of member i , respectively. The available funds for the PMO are expressed as:

$$\sum_{i \in \mathcal{U}} \sum_{t \in T} C_{i,t}^{\text{cm}} = C_{\text{surplus}} \quad (63)$$

where T is the set of time intervals that constitute the scheduling horizon; $C_{i,t}^{\text{cm}}$ is community microgrid cost of member i at time t ; and C_{surplus} is the community surplus (funds for the PMO). The PMO can utilize the community surplus in various ways. It may adjust the differences between buying and selling prices to generate personal income or investment. Additionally, the surplus can cover community microgrid costs such as operational expenses or distribute additional benefits to members.

Equation (64) caps the total cost for community microgrid members, ensuring that it does not surpass the traditional

cost of scheduling energy solely with retailers.

$$\sum_{i \in \mathcal{U}} C_{i,t} \leq \sum_{i \in T_m} P_{i,t}^b \pi_t^{\text{gb}} - \sum_{i \in T_m} P_{i,t}^s \pi_t^{\text{gs}} \quad \forall i \in \mathcal{U} \quad (64)$$

where T_m is the set of monthly settlement time intervals. The problem in this stage is an optimization task, where the allocation coefficients $\lambda_{i,t}^b$, $\lambda_{i,t}^s$, $\mu_{i,t}^b$ and $\mu_{i,t}^s$ are the decision variables. The objective is to minimize the discrepancy between the actual monthly operational cost and the predicted cost from Stage I, which is expressed as:

$$\begin{cases} \min_{\lambda_{i,t}^b, \lambda_{i,t}^s, \mu_{i,t}^b, \mu_{i,t}^s} \sum_{i \in \mathcal{U}} \left(\frac{\sum_{t \in T_m} C_{i,t}^{\text{DA}} - C_{i,t}}{\sum_{t \in T_m} C_{i,t}^{\text{DA}}} \right)^2 \\ \text{s.t. (1)-(4), (42)-(44), (52)-(61), (63), (64)} \end{cases} \quad (65)$$

where $C_{i,t}^{\text{DA}}$ is the expected total cost for member i at time t in the day-ahead stage.

IV. MODEL SOLUTION

The previous section outlines the proposed multi-stage optimization strategy for community microgrid, including the associated optimization objective functions and constraints. This section details the distributed optimization algorithm used to address these problems. The distributed algorithm accommodates differences among members and adapts to varying numbers of participants. Moreover, it ensures privacy and security, as the PMO relies on current measurements from smart meters and carbon emission data from sensors.

To address the aforementioned problems, this paper adopts the ADMM algorithm, a distributed algorithm that solves the augmented Lagrangian function through iterative updates of local solutions, global coordinations, and dual variables [31].

The objective functions of members for Stages I and II, given by (41) and (51), respectively, can be reformulated in the following augmented Lagrangian form, where κ is the iteration index.

$$\begin{cases} \min_{\mathbf{x}_i^{\text{DA}(\kappa)}} \left[(1 - L_i) f_i^{\text{DA}} + L_i C_i^{\text{GlueVar}} + \frac{\rho}{2} \|\mathbf{x}_i^{\text{DA}(\kappa)} - \mathbf{X}_i^{\text{DA}(\kappa-1)}\|_2^2 + \gamma_i^{\text{DA}(\kappa-1)} (\mathbf{x}_i^{\text{DA}(\kappa)} - \mathbf{X}_i^{\text{DA}(\kappa-1)}) \right] \\ \text{s.t. (1), (9)-(22), (25)-(28), (35)-(40)} \end{cases} \quad (66)$$

$$\begin{cases} \min_{\mathbf{x}_i^{\text{RT}(\kappa)}} \left[f_i^{\text{RT}} + \gamma_i^{\text{RT}(\kappa-1)} (\mathbf{x}_i^{\text{RT}(\kappa)} - \mathbf{X}_i^{\text{RT}(\kappa-1)}) + \frac{\rho}{2} \|\mathbf{x}_i^{\text{RT}(\kappa)} - \mathbf{X}_i^{\text{RT}(\kappa-1)}\|_2^2 \right] \\ \text{s.t. (9)-(24), (46)} \end{cases} \quad (67)$$

where κ is the iteration index of the ADMM algorithm; ρ is the penalty parameter of the augmented Lagrangian function; and $\gamma_i^{\text{DA}(\kappa-1)}$ and $\gamma_i^{\text{RT}(\kappa-1)}$ are the day-ahead and real-time dual variables of member i at iteration $\kappa-1$, respectively.

After the members complete their local optimizations, the PMO collects all variables $\mathbf{x}_i^{(\kappa)}$ to solve the global problem f_g and update the global variables $\mathbf{X}^{(\kappa)}$:

$$\begin{cases} \min_{\mathbf{x}_i^{(k)}} \left[f_g + \sum_{i \in \mathcal{U}} \gamma_i^{(k-1)} (\mathbf{x}_i^{(k)} - \mathbf{X}_i^{(k-1)}) + \frac{\rho}{2} \|\mathbf{x}_i^{(k)} - \mathbf{X}_i^{(k-1)}\|_2^2 \right] \\ \text{s.t. Community microgrid constraints} \end{cases} \quad (68)$$

Figure 2 illustrates the refined flowchart of the ADMM algorithm, highlighting key decision points and coordination within the community microgrid. In this algorithm, each community microgrid member solves their own local problems independently based on personalized objectives. These local problems are updated using the dual variables, penalty factors, and convergence criteria initialized at the beginning of the process.

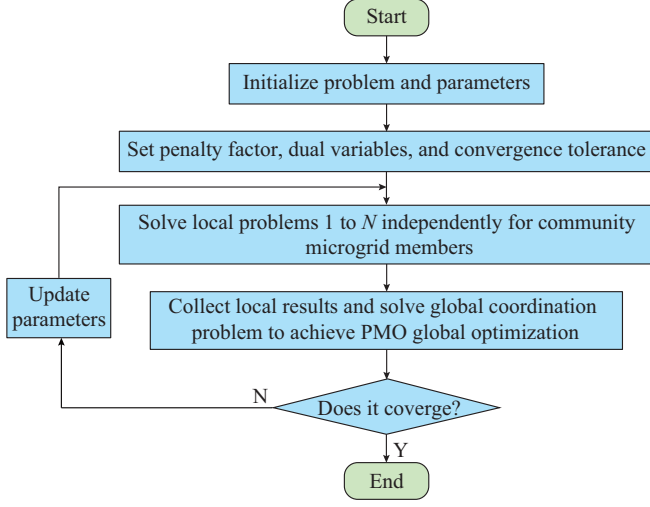


Fig. 3. Flowchart of ADMM algorithm.

After solving their problems, all members submit their optimized variables to the PMO, which performs a global coordination step by solving a centralized problem that integrates the results and enforces consensus across the network. This global step ensures compatibility with power flow constraints, voltage safety limits, and balance requirements. Once global coordination is completed, the PMO verifies convergence. If the convergence is not achieved, the dual and local variables are updated accordingly, and the process iterates.

This process provides the foundation for the settlement in Stage III. The optimized results from the ADMM algorithm in Stages I and II, including energy schedules, carbon allocations, and real-time adjustments, form the basis of calculating marginal contributions. Also, these results ensure that the VCG mechanism is grounded in validated operational outcomes, enabling fair and incentive-compatible settlements.

Since Stage III aims to minimize the deviations between actual billing and operational costs in day-ahead stage, it is sufficient to directly solve (65) without requiring a distributed algorithm.

V. CASE STUDIES

The multi-stage strategy for community microgrid proposed in this paper is applied to the IEEE European low-voltage (LV) test feeder with 55 community microgrid members [32], as shown in Fig. 4.

The load power factor is assumed to be a constant 0.95 in

this paper. Distributed generation units have a unified power factor, with capacities varying randomly. The power generation capacity of PV units ranges from 10 kW to 20 kW, while ESS power and capacities range from 5 kW/10 kWh to 10 kW/20 kWh. The PV data are sourced from Paris, France, based on historical reanalysis datasets from the European Centre for Medium-range Weather Forecasts (ECMWF) and the National Aeronautics and Space Administration (NASA).

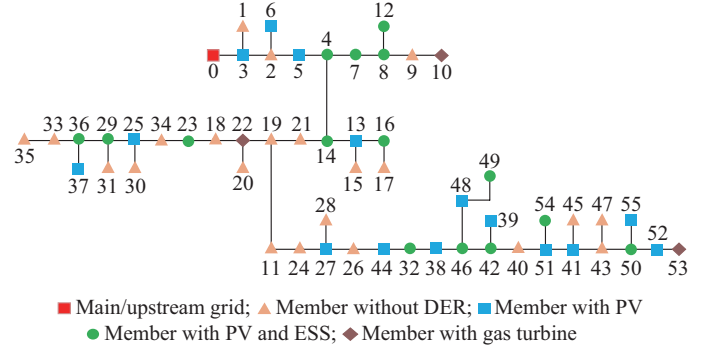


Fig. 4. IEEE European LV test feeder with 55 community microgrid members.

In all cases, electricity bought by community microgrid members from the retailer π_i^{gb} follows time-of-use (ToU) pricing: peak-hour prices are at 11.75 c€/kWh and off-peak-hour prices are at 7.97 c€/kWh. The selling price to the retailer π_i^{gs} is 6.5 c€/kWh. Within the community microgrid, the electricity prices are 7.5 c€/kWh for buying and 7 c€/kWh for selling. While the carbon quotas are relatively stable, the prices are at 7.2 c€/kg for buying and 6.7 c€/kg for selling. Based on the contract prices of the EU Emissions Trading System, the buying price from the retailer is 8.4 c€/kg, and the selling price is 6.2 c€/kg.

This section develops five distinct PV power output scenarios to comprehensively analyze the PV uncertainties, as illustrated in Fig. 5. These scenarios are generated through a two-step method: first, Monte-Carlo simulation based on historical PV data creates a wide range of possible profiles of PV power output; then, K-means clustering is applied to identify five representative scenarios. The first scenario models typical clear weather conditions with minor fluctuations and stable PV power output. The other four scenarios incorporate increasing degrees of fluctuations, simulating varying weather conditions such as cloud cover and overcast conditions. This two-step method ensures that the selected scenarios comprehensively capture the instability of practical PV power output and support the development of robust trading and risk management strategies.

This section compares several cases of the proposed multi-stage optimization strategy.

1) Case 1 is the traditional strategy that focuses solely on electricity without GlueVaR, using proportional allocation based on contribution.

2) Case 2 includes carbon alongside electricity but does not use GlueVaR for PV risk, with proportional allocation based on contribution.

3) Case 3 expands on Case 2 by replacing proportional allocation with the VCG mechanism.

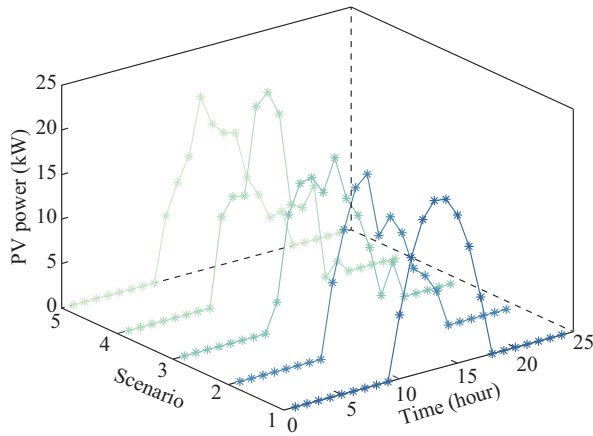


Fig. 5. PV power output scenarios.

4) Case 4 expands on Case 3 by incorporating both electricity and carbon using the VCG-based allocation method and considering multiple PV power output scenarios with GlueVaR for risk management in Stage I.

5) Case 5 employs stochastic programming for risk management in Stage I to manage the PV uncertainties, using the VCG mechanism in Stage III.

6) Case 6 uses robust optimization for risk management in Stage I to address the PV uncertainties, also adopting the VCG mechanism in Stage III.

A. Convergence Analysis

All simulation is conducted on a computer with an Intel Core i7-12700H processor and 16 GB of memory. The model code, developed in MATLAB R2020b, is solved using Gurobi 11.01.

Table I shows that including carbon results increases solution time in Stage I compared with focusing solely on electricity scheduling. Additionally, considering multiple scenarios further extends iteration time. However, Stage II is completed faster than Stage I, satisfying real-time operation requirements. Parallel computing tools are used to enhance computation speed and efficiency for both stages.

TABLE I
ITERATION TIME

Case	Iteration time (s)		
	Stage I	Stage II	Stage III
1	68.014	294.127	348.951
2	112.165	294.127	348.951
3	112.165	294.127	567.442
4	236.243	387.481	567.442

Figure 6 illustrates the iterative convergence of primal and dual residuals in Stage I of Case 4. After 15 iterations, both primal and dual residuals closely align and approach zero, confirming the convergence requirements of the ADMM algorithm.

B. Economic Analysis

Figure 7 illustrates the allocation of electricity within the

community microgrid different in Case 4 on a particular day, where the different colors represent community microgrid members. Most electricity scheduling occurs during the daytime when PV output is high, while members with gas turbines provide a baseline electricity supply. After 18:00, PV output decreases, but electricity consumption rises due to the evening peak, prompting gas turbines to ramp up output. Additionally, members with ESSs begin discharging to maintain voltage stability.

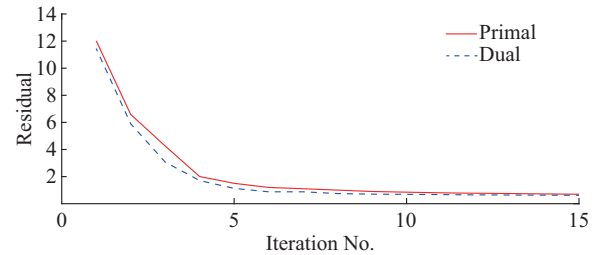


Fig. 6. Iterative convergence of primal and dual residuals in Stage I of Case 4.

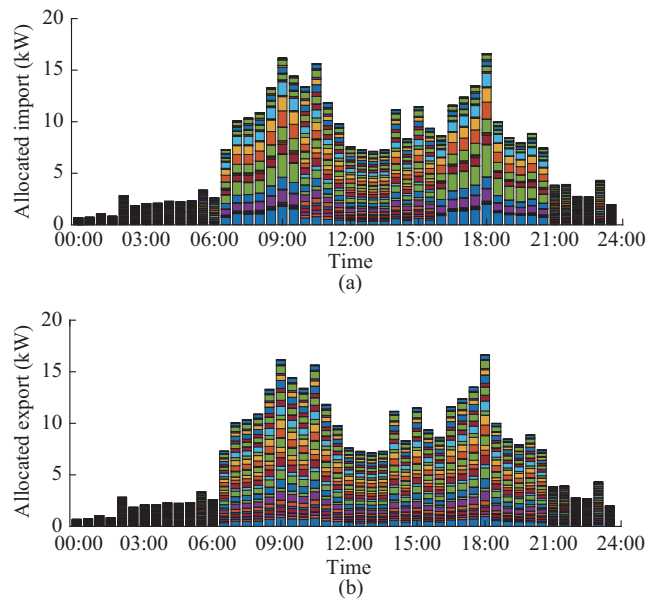


Fig. 7. Allocation of electricity within community microgrid in Case 4 on a particular day. (a) For buyers. (b) For sellers.

Figure 8(a) compares the total costs and revenues of community microgrid members across six different cases. Compared with Case 1, which involves only electricity scheduling, the inclusion of carbon quota allocation in subsequent cases raises both costs and revenues, significantly increasing the overall profit. Compared with Case 2, the VCG mechanism in Case 3 promotes more accurate reporting of information, enhancing the overall welfare and boosting the revenue. Case 4, which incorporates GlueVaR, enables community microgrid members to manage risks more effectively, leading to a slight reduction in costs, a modest increase in revenue, and an overall increase in profit of about 8%. Compared with alternative risk management methods, Case 4 demonstrates superior performance: it achieves higher revenues than Case 5 while avoiding the excessive conservatism in

Case 6, which shows the highest costs but relatively lower revenues.

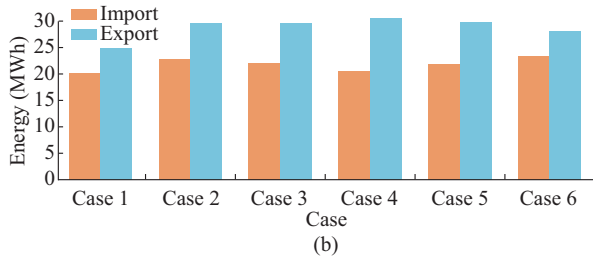
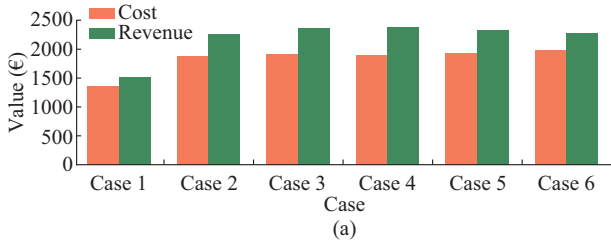


Fig. 8. Cost, revenue, and energy in different cases. (a) Total cost and revenue of community microgrid members. (b) Energy import and export.

Figure 8(b) illustrates a substantial increase in total electrical energy when carbon is introduced. This development is due to the carbon incentives for community microgrid members with renewable energy sources, boosting renewable generation. Consequently, more electricity becomes available for sale both in the community microgrid and the external grid. Additionally, by accounting for the PV uncertainties and extreme scenarios, community microgrid members can better adjust their generation strategies, improving the risk management.

C. Carbon Quota Allocation Analysis

Figure 9 provides a detailed view of the carbon repartition coefficients on a specific day. Figure 9(a) shows that gas turbine units progressively increase their output from early morning, with a notable rise during peak periods to meet the load demand, leading to higher carbon quota requirements. Conversely, Fig. 9(b) demonstrates that PV units can sell carbon quotas. Consequently, during peak periods, PV units sell carbon quotas within the community microgrid to both gas turbine units and external buyers, enhancing the revenue.

Figure 10 depicts the import and export of carbon quotas in different cases. In Case 1, which excludes carbon emissions, the values for both buying and selling are zero. In Case 3, the VCG mechanism promotes increased sales by fostering more honest transactions across the community. Additionally, in Case 4, where GlueVaR is used to manage risk, members manage uncertainties more effectively, leading to further increases in earnings compared with Cases 2 and 3. Cases 5 and 6 show intermediate performance in carbon quota trading, with Case 5 demonstrating moderate trading volumes, while Case 6 exhibits more conservative carbon quota transactions due to its risk-averse management.

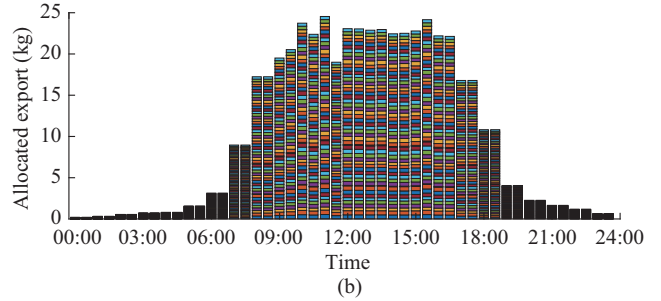
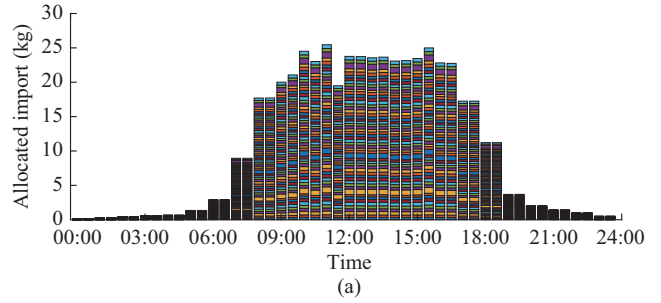


Fig. 9. Carbon repartition coefficients on a specific day. (a) For buyers. (b) For sellers.

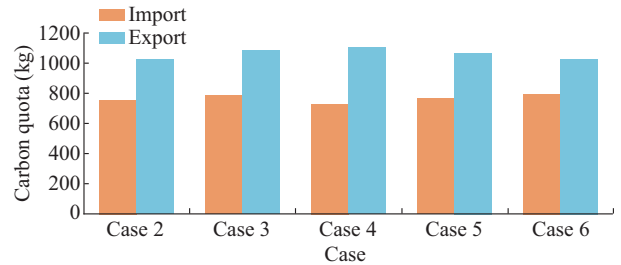


Fig. 10. Import and export of carbon quotas in different cases.

D. Risk Management Analysis

Figure 11 illustrates total cost and GlueVaR under different risk preferences L for each community microgrid member. Figure 12 presents the relationship between total cost and GlueVaR under different risk preferences L . Each red marker corresponds to the average value of all 55 community microgrid members under a specific L , and the vertical error bars depict the variability in cost among members. As L increases, indicating stronger risk aversion, the corresponding GlueVaR decreases, reflecting improved protection against extreme events. However, this also leads to a higher value of total cost. In contrast, lower values of L reflect more risk-tolerant behavior, resulting in increased GlueVaR but reduced costs. The inclusion of error bars captures the diversity of member responses, highlighting that cost-risk outcomes vary across the community even under the same risk preference setting due to differing resource configurations and operational behaviors.

Table II presents comparative results obtained by different weights under the commonly used confidence levels $\alpha=0.9$ and $\beta=0.95$, which capture moderate fluctuations and more extreme tail risks in power system and financial risk management, respectively.

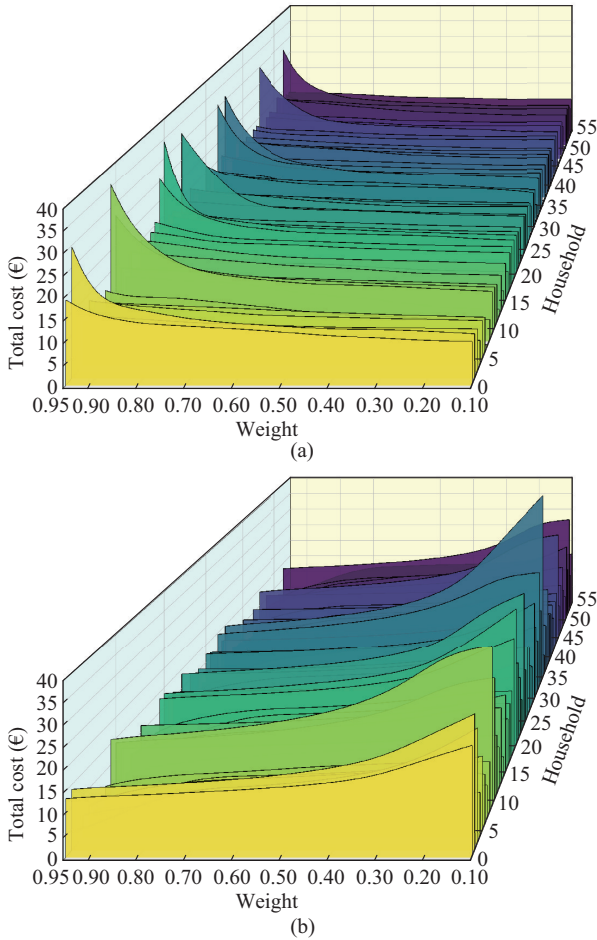


Fig. 11. Total cost and GlueVaR under different risk preferences L . (a) Total cost. (b) GlueVaR.

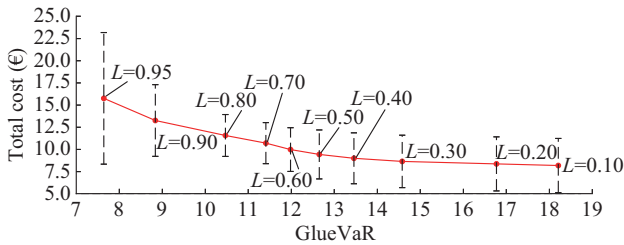


Fig. 12. Relationship between total cost and GlueVaR under different risk preferences L .

TABLE II
COMPARATIVE RESULTS OBTAINED BY DIFFERENT WEIGHTS

Risk measure	ω_1	ω_2	ω_3	Risk value
VaR_α	0.00	0.00	1.00	2015.62
$CVaR_\alpha$	0.00	1.00	0.00	2325.75
$CVaR_\beta$	1.00	0.00	0.00	2095.37
GlueVaR	0.40	0.40	0.20	2240.51
GlueVaR	0.33	0.33	0.33	2155.16
GlueVaR	0.50	0.40	0.10	2375.83

Unlike traditional CVaR methods that rely on a single confidence level, GlueVaR integrates multiple risk perspectives within a coherent method, offering greater flexibility to bal-

ance typical and extreme PV uncertainties. When only $CVaR_\beta$ is used, the risk estimate reaches 2095.37, indicating a conservative but potentially rigid method. In contrast, relying solely on $CVaR_\alpha$ produces a higher estimate of 2325.75, which captures broader uncertainties but focuses less on extremes. The lowest risk of 2015.62 arises from relying only on VaR_α , while the highest value of 2375.83 appears in a mixed scheme dominated by $CVaR_\beta$ and $CVaR_\alpha$ with weights of 0.5 and 0.4, respectively. An equal-weight scenario across the three risk measures yields a moderate estimate of 2155.16. These results suggest that greater emphasis on CVaR produces more conservative risk management, whereas stronger reliance on VaR can lead to lower but potentially underestimated risks.

E. Voltage Security Analysis

Figure 13(a) illustrates the voltage profiles for all community microgrid members in the real-time stage, while Fig. 13(b) focuses on a specific community microgrid member. The data show that node voltages of members remain within the safe upper and lower limits, demonstrating that the real-time adjustment effectively maintains voltage near the upper threshold.

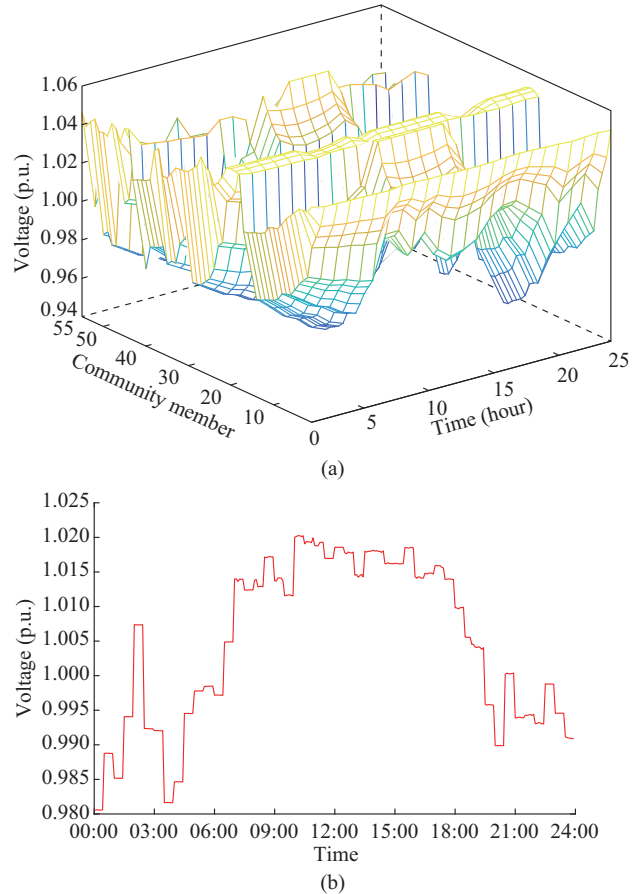


Fig. 13. Voltage profiles. (a) For all community microgrid members. (b) For a specific community microgrid member.

Figure 14 depicts the SOC of ESS for a specific day. The SOC follows a preset trajectory with a tolerance margin of $\pm\delta_{SOC}$ and remains consistently within the allowable range

of 20%-100%. The ESS units are configured with power capacities between 5 kW and 10 kW and energy capacities ranging from 10 kWh to 20 kWh, operating under a round-trip efficiency of 95%. This configuration allows the ESS to dynamically respond to power fluctuations. The SOC profile implicitly reflects the charging and discharging processes, preventing overcharging or over-discharging and enhancing voltage regulation and system stability, particularly during peak demand periods.

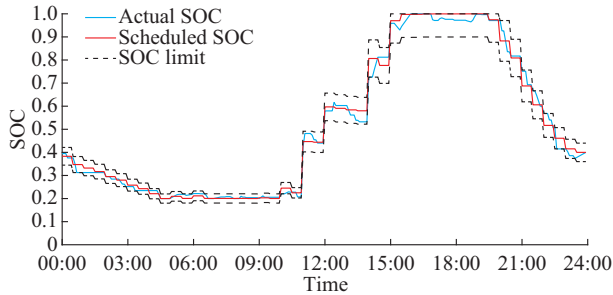


Fig. 14. SOC of ESS for a specific day.

F. Fairness Analysis of VCG Mechanism

To assess the effectiveness of the VCG mechanism in ensuring fairness and improve overall welfare, this subsection employs Jain's fairness index to measure allocation fairness.

Reference [28] shows that Jain's fairness index ranges from 0 to 1, with higher values signifying greater fairness. Table III demonstrates that the VCG-based allocation method achieves the highest fairness scores of 0.71561 for import and 0.64314 for export, outperforming other cooperative game methods including Shapley value, nucleolus, and Nash bargaining methods. This superior performance highlights the effectiveness of VCG mechanism in eliminating fraudulent behaviors and promoting fairness through its inherent incentive compatibility, which ensures truthful reporting as the dominant strategy for all participants.

TABLE III
JAIN'S FAIRNESS INDEX

Method	Jain's fairness index	
	Import	Export
Proportional	0.42582	0.39651
Shapley value	0.64892	0.61573
Nucleolus	0.61247	0.58394
Nash bargaining	0.57428	0.54836
VCG-based	0.71561	0.64314

VI. CONCLUSION

This paper proposes a multi-stage optimization strategy of community microgrid considering fair allocation and risk management, based on the VCG mechanism and GlueVaR. The proposed strategy optimizes the energy consumption and carbon emissions of the community by integrating carbon into the traditional CSC framework to enhance the total welfare. It considers multiple PV units to address uncertainties and employs GlueVaR to quantify risks arising from PV

fluctuations, offering a more flexible and comprehensive method for decision-making under risks. Additionally, the VCG mechanism is used in the final stage to allocate revenues fairly and mitigate fraudulent behaviors. Case study analysis verifies the following conclusions.

1) By introducing the Jain's fairness index to measure fairness, the VCG mechanism significantly reduces fraudulent behaviors by incentivizing members to report their energy supply and demand honestly. This enhances fairness in transactions, improves the overall community welfare effectively, and reinforces the system stability, ensuring the long-term sustainability of community energy sharing.

2) The GlueVaR method offers a flexible and comprehensive way to manage PV uncertainties by incorporating multiple confidence levels for assessing both average and extreme risks. By tuning risk preference parameters, community microgrid members can balance cost and risk, improving individual outcomes and the overall community welfare.

3) The improved CSC framework increases income for renewable energy members. By combining carbon with local energy sharing, it promotes renewable energy sharing and more efficient consumption of energy. In addition, it is capable of contributing to the sustainable growth of the community energy systems.

REFERENCES

- [1] B. Liu, D. Wang, J. Zhu *et al.*, "A rule-based bionic energy management system for grid-connected community microgrid using peer-to-peer trading with rapid settlement," *IEEE Transactions on Sustainable Energy*, vol. 15, no. 1, pp. 215-235, Jan. 2024.
- [2] L. Li, S. Fan, J. Xiao *et al.*, "Energy management strategy for community prosumers aggregated VPP participation in the ancillary services market based on P2P trading," *Applied Energy*, vol. 384, p. 125472, Apr. 2025.
- [3] G. A. H. Laugs, R. M. J. Benders, and H. C. Moll, "Maximizing self-sufficiency and minimizing grid interaction: combining electric and molecular energy storage for decentralized balancing of variable renewable energy in local energy systems," *Renewable Energy*, vol. 229, p. 120703, Aug. 2024.
- [4] S. Dorahaki, M. Rashidinejad, S. F. Fatemi Ardestani *et al.*, "An integrated model for citizen energy communities and renewable energy communities based on clean energy package: a two-stage risk-based approach," *Energy*, vol. 277, p. 127727, Aug. 2023.
- [5] Y. Zhang, V. Robu, S. Cremers *et al.*, "Modelling the formation of peer-to-peer trading coalitions and prosumer participation incentives in transactive energy communities," *Applied Energy*, vol. 355, p. 122173, Feb. 2024.
- [6] T. Capper, A. Gorbacheva, M. A. Mustafa *et al.*, "Peer-to-peer, community self-consumption, and transactive energy: a systematic literature review of local energy market models," *Renewable and Sustainable Energy Reviews*, vol. 162, p. 112403, Jul. 2022.
- [7] M. A. Putratama, R. Rigo-Mariani, A. D. Mustika *et al.*, "A three-stage strategy with settlement for an energy community management under grid constraints," *IEEE Transactions on Smart Grid*, vol. 14, no. 2, pp. 1505-1514, Mar. 2023.
- [8] X. Zhou, B. Wang, Q. Guo *et al.*, "Bidirectional privacy-preserving network-constrained peer-to-peer energy trading based on secure multiparty computation and blockchain," *IEEE Transactions on Power Systems*, vol. 39, no. 1, pp. 602-613, Jan. 2024.
- [9] Z. Liu, B. Huang, Y. Li *et al.*, "Pricing game and blockchain for electricity data trading in low-carbon smart energy systems," *IEEE Transactions on Industrial Informatics*, vol. 20, no. 4, pp. 6446-6456, Apr. 2024.
- [10] W. Vickrey, "Counterspeculation, auctions, and competitive sealed tenders," *The Journal of Finance*, vol. 16, no. 1, p. 8, Mar. 1961.
- [11] E. H. Clarke, "Multipart pricing of public goods," *Public Choice*, vol. 11, no. 1, pp. 17-33, Sept. 1971.
- [12] T. Groves, "Incentives in teams," *Econometrica*, vol. 41, no. 4, p.

- 617, Jul. 1973.
- [13] Y. Wu, C. Liu, Z. Lin *et al.*, "Vickrey-Clark-Groves-based method for eradicating deceptive behaviors in demand response transactions," *Journal of Modern Power Systems and Clean Energy*, vol. 12, no. 4, pp. 1260-1271, Jul. 2024.
- [14] L. Makowski and J. M. Ostroy, "Vickrey-Clarke-Groves mechanisms and perfect competition," *Journal of Economic Theory*, vol. 42, no. 2, pp. 244-261, Aug. 1987.
- [15] A. Shirsat, V. Muthukaruppan, R. Hu *et al.*, "A secure and adaptive hierarchical multi-timescale framework for resilient load restoration using a community microgrid," *IEEE Transactions on Sustainable Energy*, vol. 14, no. 2, pp. 1057-1075, Apr. 2023.
- [16] H. Han, X. Jiang, S. Zhang *et al.*, "A risk-based scheduling optimization strategy with explainability enhanced multi-scenario photovoltaic forecasting," *Electric Power Systems Research*, vol. 246, p. 111729, Sept. 2025.
- [17] G. Li, Q. Li, Y. Liu *et al.*, "A cooperative Stackelberg game based energy management considering price discrimination and risk assessment," *International Journal of Electrical Power & Energy Systems*, vol. 135, p. 107461, Feb. 2022.
- [18] Z. Wei, H. Xu, S. Chen *et al.*, "Learning-aided distributionally robust optimization of DC distribution network with buildings to the grid," *Sustainable Cities and Society*, vol. 113, p. 105649, Oct. 2024.
- [19] G. A. H. Laugs, R. M. J. Benders, and H. C. Moll, "Maximizing self-sufficiency and minimizing grid interaction: combining electric and molecular energy storage for decentralized balancing of variable renewable energy in local energy systems," *Renewable Energy*, vol. 229, p. 120703, Aug. 2024.
- [20] C. Wu, Y. Zhou, and J. Wu, "Two-layer data-driven robust scheduling for industrial heat loads," *Journal of Modern Power Systems and Clean Energy*, vol. 13, no. 1, pp. 265-275, Jan. 2025.
- [21] H. Han, L. Yu, Y. Zhou *et al.*, "Two-stage robust co-optimization of energy and reserve scheduling for resilient distribution systems considering line reinforcement," *Energy*, vol. 316, p. 134600, Feb. 2025.
- [22] H. Huang, G. Sun, S. Chen *et al.*, "Peer-to-peer energy trading of hydrogen-producing prosumers in power distribution network," *Sustainable Energy Technologies and Assessments*, vol. 75, p. 104221, Mar. 2025.
- [23] Y. Zeng, Q. Zhang, S. You *et al.*, "Bilayered real-time energy management strategy for hybrid power systems in hydrogen fuel cell vessels," *IEEE Transactions on Transportation Electrification*, vol. 10, no. 4, pp. 7954-7970, Dec. 2024.
- [24] H. Shuai, F. Li, J. Zhu *et al.*, "Hydroclimate-coupled framework for assessing power system resilience under summer drought and climate change," *Renewable and Sustainable Energy Reviews*, vol. 213, p. 115397, May 2025.
- [25] J. Zhong, Y. Zhao, and Y. Cao, "Collaborative optimization for energy hub and load aggregator considering the carbon intensity-driven and uncertainty-aware," *Energy*, vol. 312, p. 133546, Dec. 2024.
- [26] X. Sheng, S. Lin, W. Liang *et al.*, "Optimal long-term planning of CCUS and carbon trading mechanism in offshore-onshore integrated energy system," *Applied Energy*, vol. 379, p. 124983, Feb. 2025.
- [27] A. N. Madavan, N. Dahlin, S. Bose *et al.*, "Risk-based hosting capacity analysis in distribution systems," *IEEE Transactions on Power Systems*, vol. 39, no. 1, pp. 355-365, Jan. 2024.
- [28] S. Leucci, A. Mamageishvili, and P. Penna, "No truthful mechanism can be better than n approximate for two natural problems," *Games and Economic Behavior*, vol. 111, pp. 64-74, Sept. 2018.
- [29] C. Huang, Q. Hu, L. Sang *et al.*, "A review of public safety power shutoffs (PSPS) for wildfire mitigation: policies, practices, models and data sources," *IEEE Transactions on Energy Markets, Policy and Regulation*, vol. 1, no. 3, pp. 187-197, Jan. 2023.
- [30] R. K. Jain, D.-M. W. Chiu, W. R. Hawe *et al.*, "A quantitative measure of fairness and discrimination," Eastern Research Laboratory, Digital Equipment Corporation, Hudson, USA, Tech. Rep. TR-301, Sept. 1984.
- [31] W. Zheng, W. Wu, B. Zhang *et al.*, "A fully distributed reactive power optimization and control method for active distribution networks," *IEEE Transactions on Smart Grid*, vol. 7, no. 2, pp. 1021-1033, Mar. 2016.
- [32] IEEE PES Test Feeder Working Group. (2016, Feb.). The IEEE European low voltage test feeder. [Online]. Available: <https://cmte.ieee.org/pes-testfeeders/resources/>

Haiteng Han received the B.S. and Ph.D. degrees from Southeast University, Nanjing, China, in 2010 and 2019, respectively. He is currently an Associate Professor with the School of Electrical and Power Engineering, Hohai University, Nanjing, China. His research interests include power system security assessment, demand response, and electricity market.

Xiangchen Jiang is currently pursuing the M.S. degree in electrical engineering with the School of Electrical and Power Engineering, Hohai University, Nanjing, China. His research interests include smart grid, integrated energy system, and electricity market.

Can Huang received the Ph.D. degree in electrical engineering from the University of Tennessee, Knoxville, USA, in 2016. He is now a Research Staff with the School of Electrical Engineering, Southeast University, Nanjing, China. His research interests include data analytics, machine learning, and their application in power and energy systems.

Chen Wu received the B.S. and M.Eng. degrees from Southeast University, Nanjing, China, in 2010 and 2013, respectively. She is currently pursuing the Ph.D. degree at Hohai University, Nanjing, China. Her research interests include power system planning and operation, demand response, and electricity market.

Sheng Chen received the B.S. and Ph.D. degrees from the College of Energy and Electrical Engineering, Hohai University, Nanjing, China, in 2014 and 2019, respectively. From January 2018 to January 2019, he was a Visiting Scholar with the Ohio State University, Columbus, USA. He is currently a Professor with the School of Electrical and Power Engineering, Hohai University. His research interests include integrated energy system and operation, and electricity market.

Qingxin Shi received the B. S. degree from Zhejiang University, Hangzhou, China, in 2011, the M.Sc. degree from University of Alberta, Edmonton, Canada, in 2014, and the Ph.D. degree from the University of Tennessee, Knoxville, USA, in 2019, where he worked as a Research Assistant Professor from 2019 to 2020. Currently, he is an Associate Professor with the School of Electrical and Electronic Engineering, North China Electric Power University, Beijing, China. His research interests include demand response, frequency regulation, and resilient urban power system.

Zhinong Wei received the B.S. degree from Hefei University of Technology, Hefei, China, in 1984, the M.S. degree from Southeast University, Nanjing, China, in 1987, and the Ph.D. degree from Hohai University, Nanjing, China, in 2004. He is currently a Professor with the School of Electrical and Power Engineering, Hohai University. His research interests include integrated energy system, power system state estimation, smart distribution system, and integration of distributed generation into power system.